Electronic Supplementary Material (ESI) for Journal of Materials Chemistry A.
This journal is © The Royal Society of Chemistry 2018

Journal of Materials Chemistry A

ARTICLE

Electronic Supplementary Information

Boosting the thermoelectric performance of misfit-layered $(SnS)_{1.2}(TiS_2)_2$ by a Co- and Cu-substituted alloying effect

Cong Yin,[a] Qing Hu,[a] Mingjing Tang,[a] Hangtian Liu,[a] Zhiyu Chen,[a] Zhengshang Wang[a] and Ran Ang*[ab]

[a] Key Laboratory of Radiation Physics and Technology, Ministry of Education, Institute of Nuclear Science and Technology, Sichuan University, Chengdu 610064, China

[b] Institute of New Energy and Low-Carbon Technology, Sichuan University, Chengdu 610065, China

*Corresponding author and E-mail: rang@scu.edu.cn

Analysis and fitting of x-ray absorption fine structure (XAFS)

The synchrotron radiation *in situ* x-ray absorption fine structure (XAFS) spectroscopy for the $(SnS)_{1.2}(TiS_2)_2$, $(SnS)_{1.2}(Co_{0.02}Ti_{0.98}S_2)_2$, and $(SnS)_{1.2}(Cu_{0.02}Ti_{0.98}S_2)_2$ samples were performed at the 1W1B beamline, utilizing the Beijing Synchrotron Radiation Facility (BSRF) of China. The data of Ti *K*-edge XAFS spectroscopy for the three samples were collected in transmission mode using ion chambers filled with nitrogen. Taking into account the low content of Co and Cu ions in the substituted samples, the data of Co and Cu *K*-edge XAFS spectroscopy were recorded in fluorescence mode using a Lytle detector to monitor the fluorescence.[1]

In order to obtain high-quality data, the raw XAFS spectroscopy with some called "glitches" have to be removed firstly via deglitching technique before further processing, and subtracting the pre-edge background, as the most desirable region in the extended XAFS (EXAFS) data, which is the region above the absorption edge, then normalizing to an edge-jump step for eliminating the difference in the samples, utilizing ATHENA module implemented in the IFEFFIT software packages.[2] Subsequently, for executing the corresponding Fourier transform (FT) function, the EXAFS data of $\chi(E)$ in the *E*-space would be switched into $\chi(k)$ in the *k*-space based on $k=[2m(E-E_0)/\hbar^2]^{1/2}$. Meanwhile, k^3-weighted $\chi(k)$ data were adopted for compensating the weakening of the waves with extended *k*. Finally, the acquired k^3-weighted EXAFS data of Ti, Co, and Cu *K*-edge would be switched into *R*-space by Fourier transform of $k^3\chi(k)$ function.

To quantitatively acquire the local structural parameters at Ti, Co, and Cu *K*-edge for the pristine, Co-, and Cu-substituted samples, least-squares fittings for the EXAFS data were performed utilizing the ARTEMIS module of IFEFFIT software packages.[2] The experimental EXAFS data is simulated by following theoretical equation.[1,3]

$$\chi(k)=\sum_j \frac{N_j S_0^2 f_j(k)}{kR_j^2}\exp[-2k^2\sigma_j^2]\exp[\frac{-2R_j}{\lambda_j(k)}]\sin[2kR_j+\delta_j(k)+2\phi_C(k)]$$

Here, N_j is the number of atoms in the j^{th} coordination shell, S_0^2 is the amplitude reduction factor, $f_j(k)$ is the effective curved-wave backscattering amplitude of the scattering atom, R_j is the distance between x-ray absorbing central atom and scattering atoms, σ_j is the Debye-Waller parameter (the variation of distances around the average R_j), $\lambda_j(k)$ is the mean free path of excited photoelectron, $\delta_j(k)$ is the scattering phase shift of scattering atom, and $\phi_C(k)$ is the phase-shift of absorbing atom, respectively. The functions of $f_j(k)$, $\lambda_j(k)$ and $\phi_C(k)$ were calculated with the *ab initio* code FEFF8.2.

It is noted that single-scattering fittings for the EXAFS data at Ti, Cu, and Co *K*-edge for the three samples were carried out in this work. The amplitude reduction factor S_0^2 was treated as fixed value obtained from the foil samples, and the obtained values are 0.54 for Ti *K*-edge, 0.70 for Cu *K*-edge, and 0.95 for Co *K*-edge, respectively. The coordination numbers *N* of the first coordination shells, interatomic distances *R*, Debye-Waller factor σ^2, and the edge-energy shift ΔE_0 were guessed as free variable. The fitting EXAFS results were in consistence with lattice parameters determined by powder x-ray diffraction (XRD) and structural Rietveld refinement,[4] demonstrating the sufficiently high precision of local atomic structure based on the EXAFS fitting. According to the above fitting procedure, the repeatable fitting results of EXAFS data are listed in Table S2 in the Supporting Information.

Supplementary Figure S1

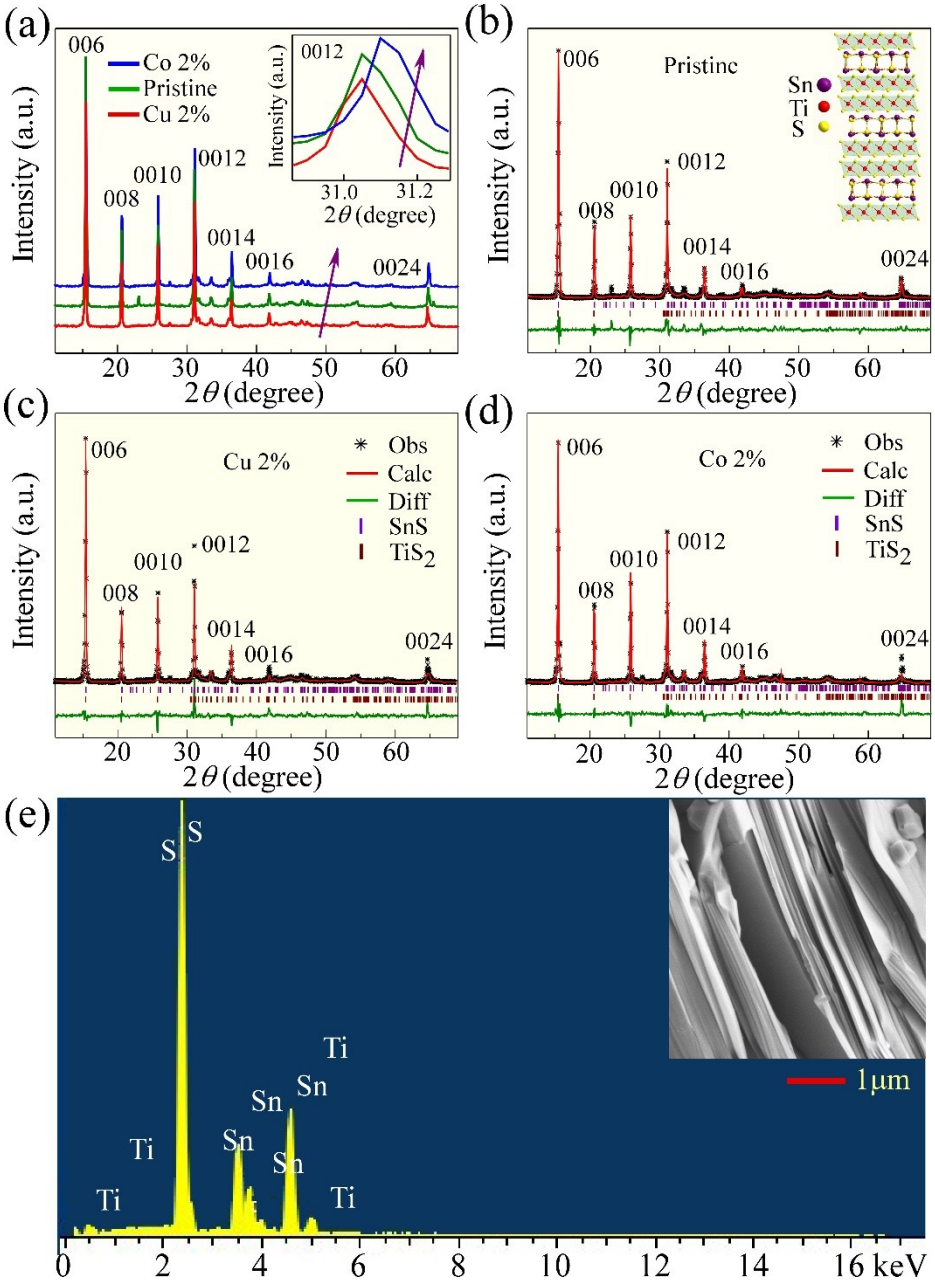

Figure S1. (a) Powder XRD patterns for the three samples. (b-d) Powder XRD patterns with the Rietveld refinement for the pristine sample $(SnS)_{1.2}(TiS_2)_2$ (b), the Cu-substituted sample $(SnS)_{1.2}(Cu_{0.02}Ti_{0.98}S_2)_2$ (c) and the Co-substituted sample $(SnS)_{1.2}(Co_{0.02}Ti_{0.98}S_2)_2$ (d). (e) The EDS patterns for the pristine sample $(SnS)_{1.2}(TiS_2)_2$. The inset of (e) SEM image showing the characteristic layered structure.

Supplementary Figure S2

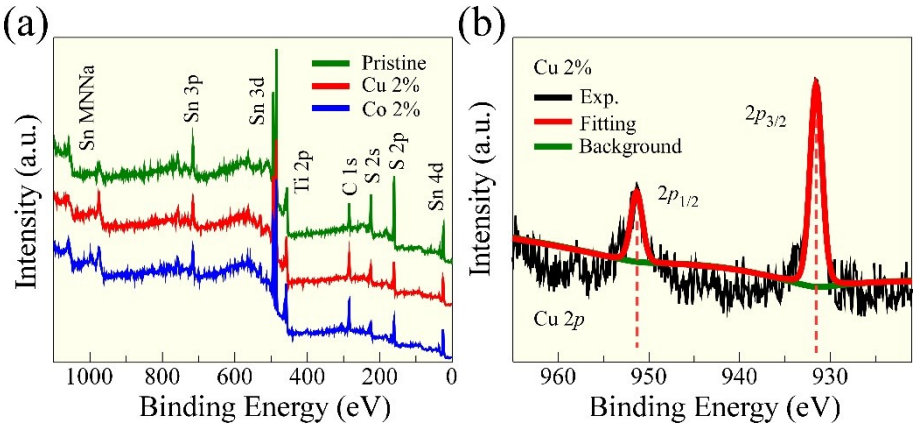

Figure S2. (a) XPS spectra for the pristine, Co-, and Cu-substituted samples. (b) XPS spectra of the Cu 2*p* regions for the Cu-substituted sample. Vertical fitting red lines demonstrate the valence of Cu^{2+} ion based on the peak positions of $2p_{1/2}$ and $2p_{3/2}$.

Supplementary Figure S3

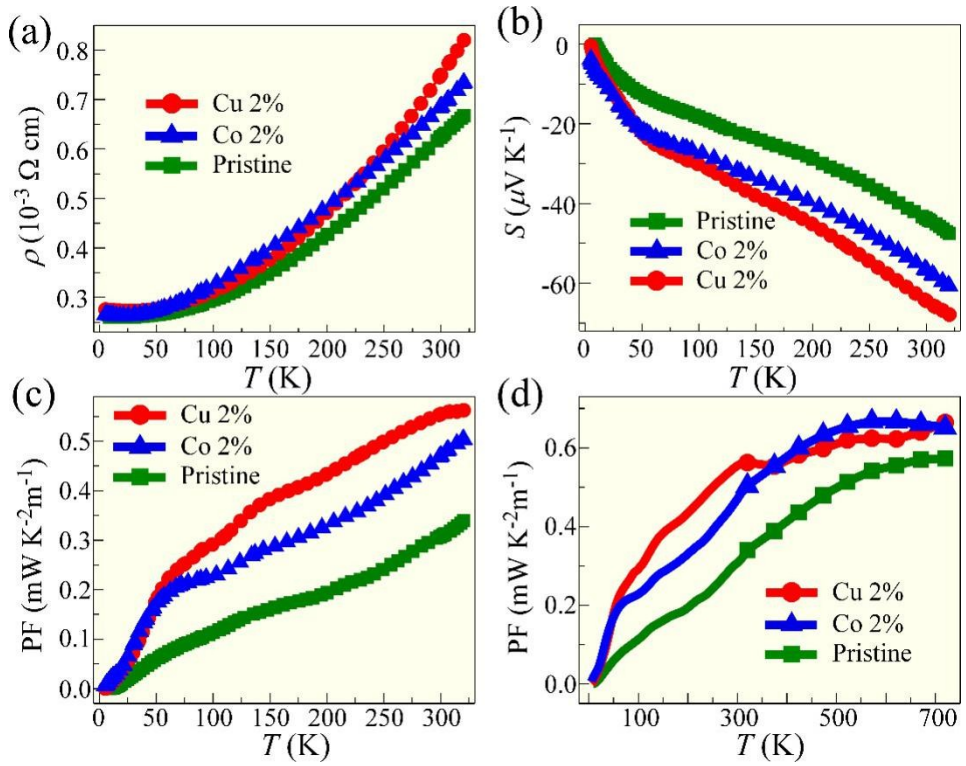

Figure S3. (a-c) Temperature dependence of resistivity ρ (a), Seebeck coefficient (b), and power factor (c) below room temperature for the pristine, Co-, and Cu-substituted samples. (d) Temperature dependence of power factor in the whole temperature range for the three samples.

Supplementary Figure S4

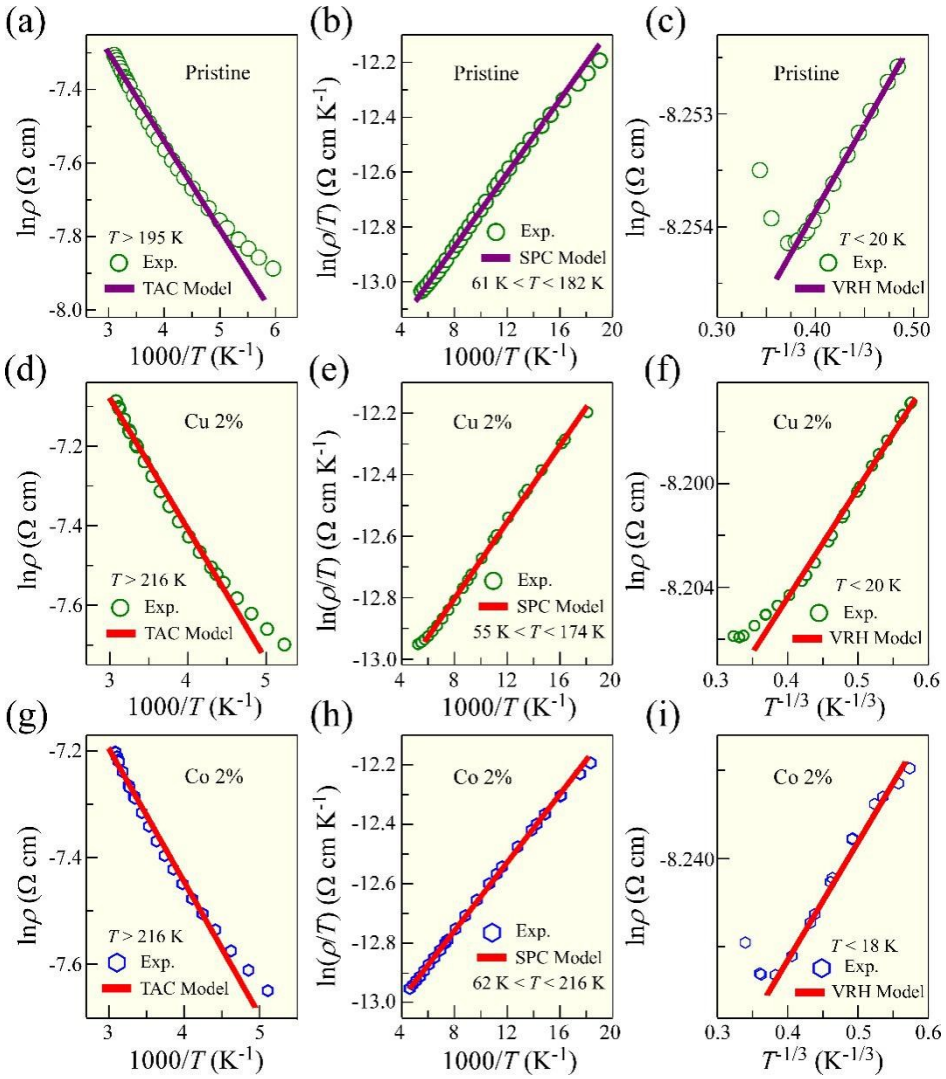

Figure S4. (a-i) Plots of lnρ against 1000/T, ln(ρ/T) against 1000/T, and lnρ against $T^{-1/3}$ for the pristine sample (a-c), the Cu-substituted sample (d-f), and the Co-substituted sample (g-i). The solid lines correspond to the fitting in the different temperature range by thermally activated conduction (TAC) model, small polaron conduction (SPC) model, and variable-range-hopping (VRH) model, respectively.

Supplementary Figure S5

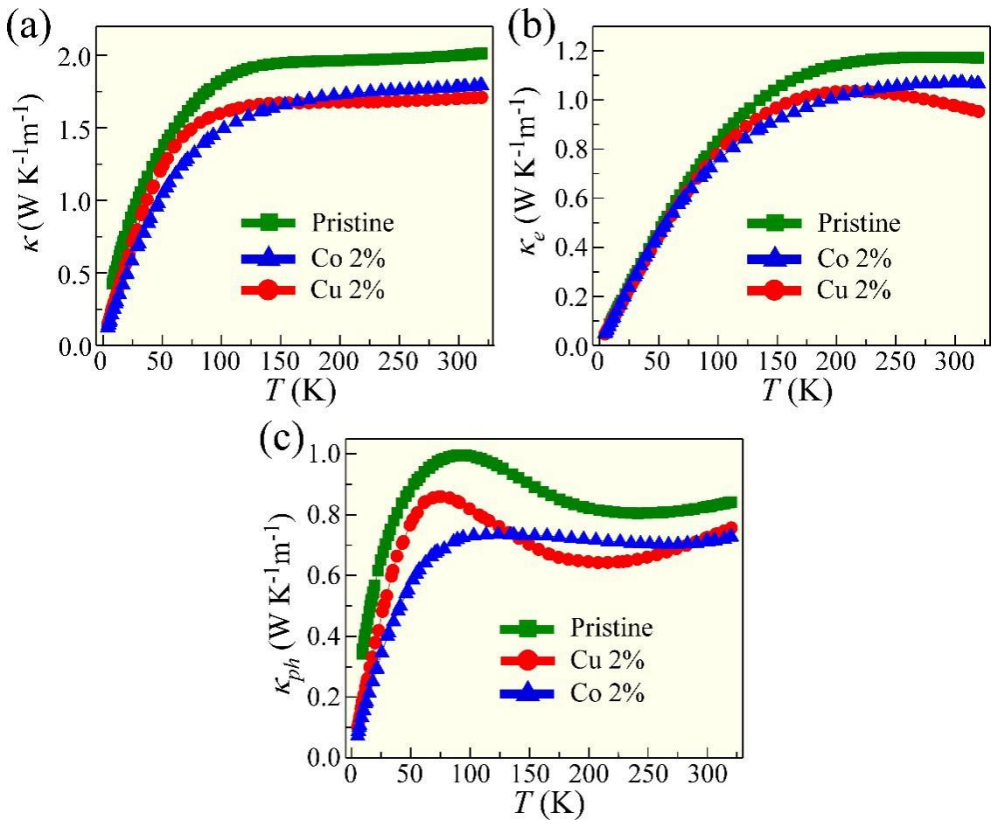

Figure S5. (a-c) Temperature dependence of total thermal conductivity κ (a), electrical thermal conductivity κ_e (b), and phononic thermal conductivity κ_{ph} (c) below room temperature for the pristine, Co-, and Cu-substituted samples.

Supplementary Table S1

Table S1. Experimental parameters from Hall measurements at room temperature. The parameters R_H, n, μ, and m^* represents the Hall coefficient, carrier concentration, carrier mobility, and effective mass, respectively. Evidently, the optimal sample is for the Cu substitution.

Parameters (320 K)	R_H 10^{-9} (m^3 C^{-1})	n 10^{21} (cm^{-3})	μ (cm^2 $V^{-1}s^{-1}$)	m^* (m_0)
$(SnS)_{1.2}(TiS_2)_2$	-2.70	2.31	4.05	3.9
$(SnS)_{1.2}(Co_{0.02}Ti_{0.98}S_2)_2$	-3.02	2.07	4.11	4.6
$(SnS)_{1.2}(Cu_{0.02}Ti_{0.98}S_2)_2$	-3.11	2.01	3.79	5.0

Supplementary Table S2

Table S2. The fitting results of EXAFS data. The parameter *N* represents the Ti-S, Co-S and Cu-S coordination, and the parameter *R* stands for the corresponding interatomic distance. The parameter σ^2 denotes the degree of disorder, and the parameter ΔE_0 is the edge energy for the pristine, Co-, and Cu-substituted samples.

Sample	Path	*N*	*R* (Å)	σ^2 (Å^2)	ΔE_0 (eV)	*R*-factor
$(SnS)_{1.2}(TiS_2)_2$	Ti-S	6.43±1.09	2.442±0.016	0.0051±0.0023	3.51±1.61	0.0176
$(SnS)_{1.2}(Co_{0.02}Ti_{0.98}S_2)_2$	Ti-S	6.44±0.85	2.413±0.015	0.0070±0.0019	3.03±2.58	0.0039
	Co-S	6.18±0.70	2.421±0.018	0.0084±0.0018	3.76±2.13	0.0019
$(SnS)_{1.2}(Cu_{0.02}Ti_{0.98}S_2)_2$	Cu-S	6.05±0.58	2.485±0.016	0.0170±0.0020	3.70±1.52	0.0047

Supplementary Table S3

Table S3. The values of dimensionless figure of merit *ZT* for all of state-of-the-art misfit-layered chalcogenides refs.[5-11] Distinctly, the value of *ZT* (~0.42) at 720 K for the Cu-substituted sample in this work is the highest in all of these compounds.

Samples	*T* (K)	*ZT*	Reference
$(BiS)_{1.2}(TiS_2)_2$	700	0.28	[5]
$(SnS)_{1.2}(TiS_2)_2$	700	0.37	[5]
$(PbS)_{1.18}(TiS_2)_2$	700	0.30	[5]
$(Bi_{0.9}Ca_{0.1}S)_{1.2}(TiS_2)_2$	750	0.24	[6]
$(BiS)_{1.2}(Mg_{0.05}Ti_{0.95}S_2)_2$	750	0.17	[6]
$(Bi_{0.9}Sr_{0.1}S)_{1.2}(TiS_2)_2$	750	0.16	[6]
$(BiS)_{1.2}(Ti_{0.975}Cr_{0.025}S_2)_2$	750	0.29	[7]
$(BiS)_{1.2}(Ti_{0.95}Cr_{0.05}S_2)_2$	750	0.25	[8]
$(LaS)_{1.20}CrS_2$	950	0.14	[9]
$(LaS)_{1.14}NbS_2$	950	0.15	[9]
$(La_{1.05}S_{1.05})_{1.14}NbS_2$	950	0.2	[10]
$Sn_{1.16}Nb(Se_{0.9}S_{0.1})_{3.16}$	760	0.03	[11]
$(SnS)_{1.2}(Cu_{0.02}Ti_{0.98}S_2)_2$	720	0.42	This work
$(SnS)_{1.2}(Co_{0.02}Ti_{0.98}S_2)_2$	720	0.35	This work

References

1 Z. H. Sun, Q. H. Liu, T. Yao, W. S. Yan, S. Q. Wei, *Sci. China Mater*. 2015, **58**, 313-341.
2 B. Ravel, M. Newville, *J. Synchrotron Radiat*. 2005, **12**, 537-541.
3 Y. J. Chen, S. F. Ji, Y. G. Wang, J. C. Dong, W. X. Chen, Z. Li, R. A. Shen, L. R. Zheng, Z. B. Zhuang, D. S. Wang, Y. D. Li, *Angew. Chem. Int. Ed*. 2017, **56**, 6937-6941.
4 C. Yin, Q. Hu, G. Y. Wang, T. Y. Huang, X. Y. Zhou, X. Zhang, Y. W. Dou, B. Kang, J. Tang, N. Liu, R. Ang, *Appl. Phys. Lett*. 2017, **110**, 043507.
5 C. L. Wan, Y. F. Wang, N. Wang, K. Koumoto, *Materials* 2010, **3**, 2606-2617.
6 Y. E. Putri, C. L. Wan, Y. F. Wang, W. Norimatsu, M. Kusunoki, K. Koumoto, *Scripta Mater*. 2012, **66**, 895-898.
7 Y. E. Putri, C. L. Wan, R. Z. Zhang, T. Mori, K. Koumoto, *J. Adv. Ceram*. 2013, **2**, 42-48.
8 Y. E. Putri, C. L. Wan, F. Dang, T. Mori, Y. Ozawa, W. Norimatsu, M. Kusunoki, K. Koumoto, *J. Electron. Mater*. 2014, **43**, 1870-1874.
9 P. Jood, M. Ohta, H. Nishiate, A. Yamamoto, O. I. Lebedev, D. Berthebaud, K. Suekuni, M. Kunii, *Chem. Mater*. 2014, **26**, 2684-2692.
10 P. Jood, M. Ohta, O. I. Lebedev, D. Berthebaud, *Chem. Mater*. 2015, **27**, 7719-7728.
11 P. Jood, M. Ohta, *Rsc Adv*. 2016, **6**, 105653-105660.